ELSEVIER

Separation and Purification Technology 29 (2002) 1–13

Separation and Purification Technology

www.elsevier.com/locate/seppur

Influence of interphase mass transfer on the composition trajectories and crossing of boundaries in ternary azeotropic distillation

P.A.M. Springer, R. Baur, R. Krishna *

Department of Chemical Engineering, University of Amsterdam, Nieuwe Achtergracht 166, 1018 WV Amsterdam, The Netherlands

Received 12 October 2000; received in revised form 12 May 2001; accepted 15 May 2001

Abstract

This paper examines the influence of mass transfer on the composition trajectories in multicomponent azeotropic distillation. Simulations were carried out for three different ternary systems: methanol–isopropanol–water, water–ethanol–acetone, and water–methanol–methylacetate. Two different models were used to calculate the composition trajectories in a tray column: an equilibrium (EQ) stage model and a rigorous nonequilibrium (NEQ) stage model based on the Maxwell–Stefan diffusion equations. The simulations show that the EQ and NEQ model trajectories could follow different composition paths and could end up in completely different corners of the composition space. Furthermore, in all the three case studies the NEQ model trajectory was found to cross the distillation boundary even when the boundary is a straight line. The study has implications for the development of improved separation strategies.

Keywords: Aazeotropic distillation; Residue curve maps; Maxwell–Stefan equations; Distillation boundary; Nonequilibrium stage; Equilibrium stage

Nomenclature

a'	interfacial area per unit volume of vapour bubble (m^2/m^3)
B_{ij}	NRTL parameters; see Table 1 (K)
c_t	mixture molar density (mol/m^3)
c_t^L	mixture molar density of the liquid phase (mol/m^3)
c_t^V	mixture molar density of the vapour phase (mol/m^3)
d_b	bubble diameter (m)
$Đ_{x,ij}$	Maxwell–Stefan diffusivity for pair i–j for the liquid phase (m^2/s)

* Corresponding author. Fax: + 31-20-5255-604

E-mail address: krishna@its.chem.uva.nl (R. Krishna).

1383-5866/02/$ - see front matter
PII: S1383-5866(01)00157-5

$Đ_{y,ij}$	Maxwell–Stefan diffusivity for pair i–j for the vapour phase (m^2/s)
E_i	component Murphree efficiency (–)
Fo	Fourier number, $Fo_{ij} \equiv 4Đ_{y,ij}\tau_v/d_b^2$ (–)
G_{ij}	NRTL parameters; see Table 1 (–)
g	acceleration due to gravity (m/s^2)
h	distance along froth height (m)
h_f	height of dispersion (m)
k_{ij}	element for matrix of multicomponent mass transfer coefficient (m/s)
$[k_x]$	matrix of multicomponent liquid mass transfer coefficients (m/s)
$[k_y]$	matrix of multicomponent vapour mass transfer coefficients (m/s)
$[K_{eq}]$	diagonal matrix of K-values (–)
$[K_{Oy}]$	matrix of multicomponent overall mass transfer coefficients (m/s)
$[NTU_{Oy}]$	matrix of overall number of vapour phase transfer units (–)
s	parameter defined in Eq. (10) (m/s)
Sh	Sherwood number (–)
t_c	liquid–bubble contact time (s)
T	Temperature (K)
V_b	single bubble rise velocity (m/s)
X_i	liquid composition for component i (–)
Y_i	vapour composition for component i (–)

Greek

α_{ij}	non-randomness parameter in NRTL equation, see Table 1 (–)
$\kappa_{x,ij}$	binary Maxwell–Stefan liquid mass transfer coefficients (m/s)
$\kappa_{y,ij}$	binary Maxwell–Stefan vapour mass transfer coefficients (m/s)
ρ_L	density of the liquid (kg/m^3)
μ_L	liquid viscosity (Pa s)
σ	surface tension (N/m)
τ_V	vapour phase residence time (s)
τ_{ij}	NRTL parameters; see Table 1 (–)
ξ	Dimensionless distance along dispersion or column height (–)

Subscript

b	referring to a bubble
f	referring to the froth
i	component number
j	component number
Oy	overall parameter referred to the vapour phase
ref	Reference
t	referring to total mixture
x	referring to the x phase (liquid)
y	referring to the y phase (vapour)

Superscript

L	referring to the liquid phase
V	referring to the vapour phase
*	referring to equilibrium state

1. Introduction

There is considerable industrial interest in the design and optimization of homogeneous and heterogeneous azeotropic distillation. This interest stems from the large number of industrial columns in operation and the potential of developing improved separation schemes so as to minimize energy consumption. Residue curve maps are commonly used in developing separation flow schemes [1–3]. The existence, location and curvature of distillation boundaries are very important in the synthesis of azeotropic distillation sequences. The curvature of the boundary has a significant impact on whether or not it is possible to cross it during distillation. In the literature [3–16] it is remarked that boundary crossing is only possible if the feed is located on the *concave* side of the distillation boundary. It is also stated in the literature that straight-line distillation boundaries cannot be crossed [9]. Most of the published literature simulation studies on the possibilities of crossing of distillation boundaries use the equilibrium (EQ) stage model. There is evidence in the published literature that experimentally measured composition profiles in distillation columns are better simulated with nonequilibrium (NEQ) stage models, in which proper account is taken of mass transfer in either fluid phase by use of the rigorous Maxwell–Stefan diffusion equations [17–27]. The Maxwell–Stefan formulation, based on the thermodynamics of irreversible processes, takes proper account of diffusional 'coupling' between the species transfers, i.e. the flux of any species depends on the driving forces of all the species present in the mixture. In a distillation column, the influence of species coupling manifests itself in significant differences in the component mass transfer efficiencies. Castillo and Towler [27] computed NEQ distillation lines for a sieve tray column and demonstrated that modest differences between the efficiencies of different components, caused by mass transfer effects, could lead to significant differences in curvature between EQ and NEQ distillation lines. They went on to show that, in some cases, differences in curvature could be exploited by the engineer in order to obtain process designs that could not be contemplated if mass transfer effects were ignored, and that some designs based solely on equilibrium models can become infeasible when mass transfer is considered.

It is the purpose of the present communication to show that the column trajectories during distillation in a tray column predicted by the NEQ model could be significantly different to that predicted by the EQ model. Futhermore, we aim to show that the NEQ column trajectories are able to cross even straight line distillation boundaries. For illustration purposes we have performed simulations of three different ternary mixtures using a bubble cap tray configuration:

1. Methanol–Isopropanol–Water
2. Water–Ethanol–Acetone
3. Water–Methanol–Methylacetate

For the three systems both straight line and curved distillation boundaries are encountered.

2. Simulation results for bubble cap tray distillation column

The operating pressure for all simulations was 101.3 kPa and the ideal gas law was used. Activity coefficients were calculated using the NRTL interaction parameters, taken from Ref. [28], specified in Table 1, and the vapour pressures were calculated using the Antoine equations. The vapour phase was assumed to be thermodynamically ideal. The column consists of 12 stages, including the total condenser (stage 1) and partial reboiler (stage 12). The column hardware details are as specified in Table 2; the specified hardware corresponds to an experimental column in operation at the University of Amsterdam; further details can be found on our website: http://ct-cr4.chem.uva.nl/distillation/.

For all three systems considered the column was operated at total reflux. For a column oper-

Table 1
NRTL parameters for binary mixtures at 101.3 kPa, taken from Ref. [28]

	B_{ij}/(K)	B_{ji}/(K)	α_{ij}/(-)
Water–methanol	594.629	−182.605	0.297
Water–isopropanol	729.2208	70.6619	0.288
Methanol–*iso*propanol	65.711	−89.7427	0.304
Water–ethanol	624.9174	−29.169	0.2937
Water–acetone	602.6252	330.4768	0.5103
Ethanol–acetone	188.8983	22.83319	0.3006
Water–methylacetate	860.2462	442.4	0.383
Methanol–methylacetate	229.9405	284.8969	1.0293

These parameters are used along with $G_{ij} = \exp(-\alpha_{ij}\tau_{ij})$ and $\tau = B_{ij}/T$.

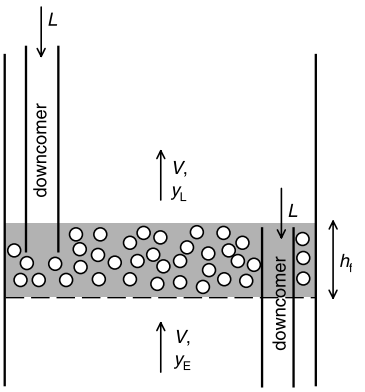

Fig. 1. Schematic of the bubble froth regime on the tray.

ated at total reflux, the reflux flow rate determines the inner flow rates of vapour and liquid phases on each stage. Simulation of total reflux operations is 'complicated' by the fact that there is no feed to the column at steady-state. To overcome this problem we specify the composition of the liquid leaving the condenser and entering the column. The simulated composition profile of the total reflux run is forced to pass through this specified composition.

All simulations were carried out using both the EQ and NEQ models. The details of the NEQ stage model are described in the earlier work of Taylor, Krishna and others [20–26]. A brief review of the model development is given below. Consider first a single stage pictured in Fig. 1. We assume that the bubble cap trays operate in the bubbly froth regime and that the bubbles are uniform in size and shape. The steady state component molar balance for 3-component distillation in tray columns is given by the 2-dimensional matrix relation

$$V_b \frac{d(y)}{dh} = [K_{Oy}](y^* - y)a' \quad (1)$$

where a' is the interfacial area per unit volume of the dispersed bubble phase and V_b is the bubble rise velocity. Eq. (1) can be re-written in terms of the overall number of transfer units for the vapour phase [NTU_{Oy}]:

Table 2
Bubble cap tray design of the laboratory-scale distillation column

Column diameter	0.0500 m	Hole pitch	0.0142 m
Tray spacing	0.0462 m	Cap diameter	0.0281 m
Number of flow passes	1	Skirt clearance	0.0030 m
Liquid flow path length	0.0308 m	Slot height	0.0050 m
Downcomer clearance	0.0039 m	Active area (of total area)	97.30%
Deck thickness	0.0030 m	Total hole area (of total area)	8.27%
Hole diameter	0.0142 m	Downcomer area (of total area)	1.35%
Weir type	Circular	Slot area	0.000221 m^2
Weir length	0.0182 m	Riser area	0.000158 m^2
Weir height	0.0092 m	Annular area	0.000462 m^2
Weir diameter	0.0058 m		

The column consists of a total of 12 stages including condenser and reboiler. There are 10 trays, each containing one bubble cap.

$$\frac{dy}{d\xi} = [NTU_{Oy}](y^* - y), \quad (2)$$

where $\xi = h/h_f$ is the dimensional distance along the froth and $[NTU_{Oy}]$ is defined as:

$$[NTU_{Oy}] \equiv \int_0^{h_f} [[K_{Oy}]a'/V_b]dh \quad (3)$$

Carrying out the integration, assuming that the matrix of overall mass transfer coefficients $[K_{Oy}]$ does not vary along the froth height, we obtain

$$[NTU_{Oy}] \equiv [K_{Oy}]a'h_f/V_b \equiv [K_{Oy}]a'\tau_V, \quad (4)$$

From Eq. (4), we see that $[NTU_{Oy}]$ can be calculated from knowledge of $[K_{Oy}]$, the interfacial area per unit volume of vapour a' and the vapour phase residence time τ_V. In our model we assume that all the bubbles to be spherical in shape with a diameter d_b. The interfacial area per unit volume of vapour a' is therefore given by:

$$a' = \frac{6}{d_b}. \quad (5)$$

The vapour residence time is determined by:

$$\tau_V = \frac{h_f}{V_b}, \quad (6)$$

where h_f is the height of dispersion (froth); this is taken to be the height of the downcomer tube above the tray floor, ie 9.2 mm. The bubble rise velocity V_b is estimated using the Mendelson equation [29], recommended by Krishna et al. [30]:

$$V_b = \sqrt{\frac{2\sigma}{\rho_L d_b} + \frac{g d_b}{2}}. \quad (7)$$

The overall matrix of mass transfer coefficients $[K_{Oy}]$ is given by the addition of resistances formula:

$$[K_{Oy}]^{-1} = [k_y]^{-1} + \frac{c_t^V}{c_t^L}[K_{eq}][k_x]^{-1}, \quad (8)$$

in which $[K_{eq}]$ represents the diagonal matrix of K-values and $[k_y]$ and $[k_x]$ are the partial transfer coefficient matrices for the vapour and liquid phases respectively.

Let us consider the matrix of the multicomponent vapour mass transfer coefficient $[k_y]$. The four elements $k_{y,ij}$ can be estimated from the mass transfer coefficients of the constituent binary pairs, $\kappa_{y,ij}$ from:

$$k_{y,11} = \kappa_{y,13}(y_1\kappa_{y,23} + (1-y_1)\kappa_{y,12})/S$$
$$k_{y,12} = y_1\kappa_{y,23}(\kappa_{y,13} - \kappa_{y,12})/S$$
$$k_{y,21} = y_2\kappa_{y,13}(\kappa_{y,23} - \kappa_{y,12})/S$$
$$k_{y,22} = \kappa_{y,23}(y_2\kappa_{y,13} + (1-y_2)\kappa_{y,12})/S \quad (9)$$

where

$$S = y_1\kappa_{y,23} + y_2\kappa_{y,13} + y_3\kappa_{y,12} \quad (10)$$

For each of the binary pairs in the mixture, the $\kappa_{y,ij}$ can be estimated from the following equation for instationary diffusion within a spherical bubble [21]:

$$Sh_{ij} \equiv \frac{\kappa_{y,ij}d_b}{Đ_{y,ij}} = \frac{2}{3}\pi^2 \left(\frac{\sum_{m=1}^{\infty} \exp\{-m^2\pi^2 Fo_{ij}\}}{\sum_{m=1}^{\infty} \frac{1}{m^2}\exp\{-m^2\pi^2 Fo_{ij}\}} \right); ij = 12,13,23 \quad (11)$$

For Fourier numbers $Fo_{ij} \equiv 4Đ_{y,ij}\tau_v/d_b^2$ larger than 0.08, the Sherwood number reduces to the asymptotic value:

$$Sh_{ij} = \frac{2\pi^2}{3} \approx 6.58; ij = 12,13,23 \quad (12)$$

For this steady-state limit, the binary vapour mass transfer coefficients are given by:

$$\kappa_{y,ij} = \frac{2\pi^2}{3}\frac{Đ_{y,ij}}{d_b}. \quad (13)$$

Eq. (13) leads to the important conclusion that $\kappa_{y,ij}$ would have an unity-power dependence on the vapour diffusivity $Đ_{y,ij}$, which is in sharp contrast with the square-root dependence for small values of Fo, small vapour phase residence times.

The matrix of the multicomponent liquid mass transfer coefficient $[k_x]$ can be obtained analogously to Eqs. (9) and (10). The binary liquid mass transfer coefficient $\kappa_{x,ij}$ can be obtained from the penetration model:

$$\kappa_{x.ij} = 2\sqrt{\frac{Đ_{x,ij}}{\pi t_c}}, \quad (14)$$

where the contact time of the liquid with gas bubbles, t_c is given by:

$$t_c = \frac{d_b}{V_b} \tag{15}$$

In the above set of model equations, the only unknown parameter is the bubble diameter d_b. Once the bubble diameter is set, the system of equations can be solved. Substituting Eq. (8) in Eq. (4) gives us the $[NTU_{Oy}]$. Assuming that the $[NTU_{Oy}]$ on a single stage is constant, Eq. (2) can be integrated using the boundary conditions

$$\begin{aligned} &\xi = 0(\text{inlet to tray})(y) = (y_E) \\ &\xi = 1(\text{outlet of tray})(y) = (y_L) \end{aligned} \tag{16}$$

to obtain the compositions leaving the distillation stage (detailed derivations are available in Ref. [21]):

$$(y^* - y_L) = \exp[-[NTU_{Oy}]](y^* - y_E) \tag{17}$$

Introducing the matrix $[Q] \equiv \exp[-[NTU_{OV}]]$, we may re-write Eq. (17) in the form

$$(y_L - y_E) = [[I] - [Q]](y^* - y_E), \tag{18}$$

where $[I]$ is the identity matrix. The limiting case of the EQ stage model is obtained when the mass transfer coefficients in either fluid phase attain large values; $[Q]$ reduces in this case to the null matrix and the compositions leaving the tray (y_L) are equal to (y^*), in equilibrium with the liquid leaving the tray.

The above set of equations model a single, NEQ, stage. More exhaustive details of this model including sample calculations for binary and ternary mixtures are available in Chap. 12 of Taylor and Krishna [21]. These equations are then incorporated into a rigorous stage-to-stage model incorporating the molar and energy balances as described in Chap. 14 of Taylor and Krishna [21].

In order to validate, and calibrate, the NEQ model for the bubble cap tray column, we carried out experiments with various binary mixtures under total reflux conditions: eight sets of experiments with ethanol–water (see Fig. 2(a) and (b)), four sets of experiments with methanol–water (see Fig. 2(c)), three sets of experiments with isopropanol–water (see Fig. 2(d)) and four sets of experiments with methanol–isopropanol (see Fig. 2(e)). All these experiments could be simulated reasonably well with the NEQ model taking a bubble size of 4.5 mm. In all the NEQ simulations for ternary mixtures, to be reported below, we assumed a bubble size $d_b = 4.5$ mm.

2.1. Methanol–isopropanol–water system

Let us consider the system: methanol (1)–isopropanol (2)–water (3) that has one binary azeotrope, as indicated in Fig. 3(a). We note that the boundary is very nearly a straight line. According to literature guidelines [9] it is not possible to cross a straight-line boundary. But these remarks regarding boundary crossing are based on the use of the EQ stage model. In order to see whether the introduction of mass transfer resistance has an influence on boundary crossing, we carried out simulations with both EQ and NEQ stage models for a 12-stage column operating at total reflux. The feed composition was chosen to be $x_1 = 0.8$, $x_2 = 0.15$ which is located in the top region *above* the distillation boundary. The EQ (cross-hair markers) and NEQ (open square markers) composition trajectories are seen to follow completely different composition trajectories; see Fig. 3(b). The NEQ model predicts that the bottom product composition corresponds to (nearly) pure water whereas the EQ model predicts the bottom product to consist of (nearly) pure isopropanol. There is experimental evidence, for total reflux in a packed distillation column [17,18] that the NEQ model predictions correspond to reality. Fig. 3(c), drawn to a different scale, clearly shows that the NEQ model crosses the distillation boundary.

Fig. 2. Experimental results (open markers) showing the column composition trajectories for various binary mixtures under total reflux conditions. Also shown are the simulation results showing the trajectories calculated by nonequilibrium (NEQ) stage model. In the NEQ model simulations a bubble size $d_b = 4.5$ mm was chosen.

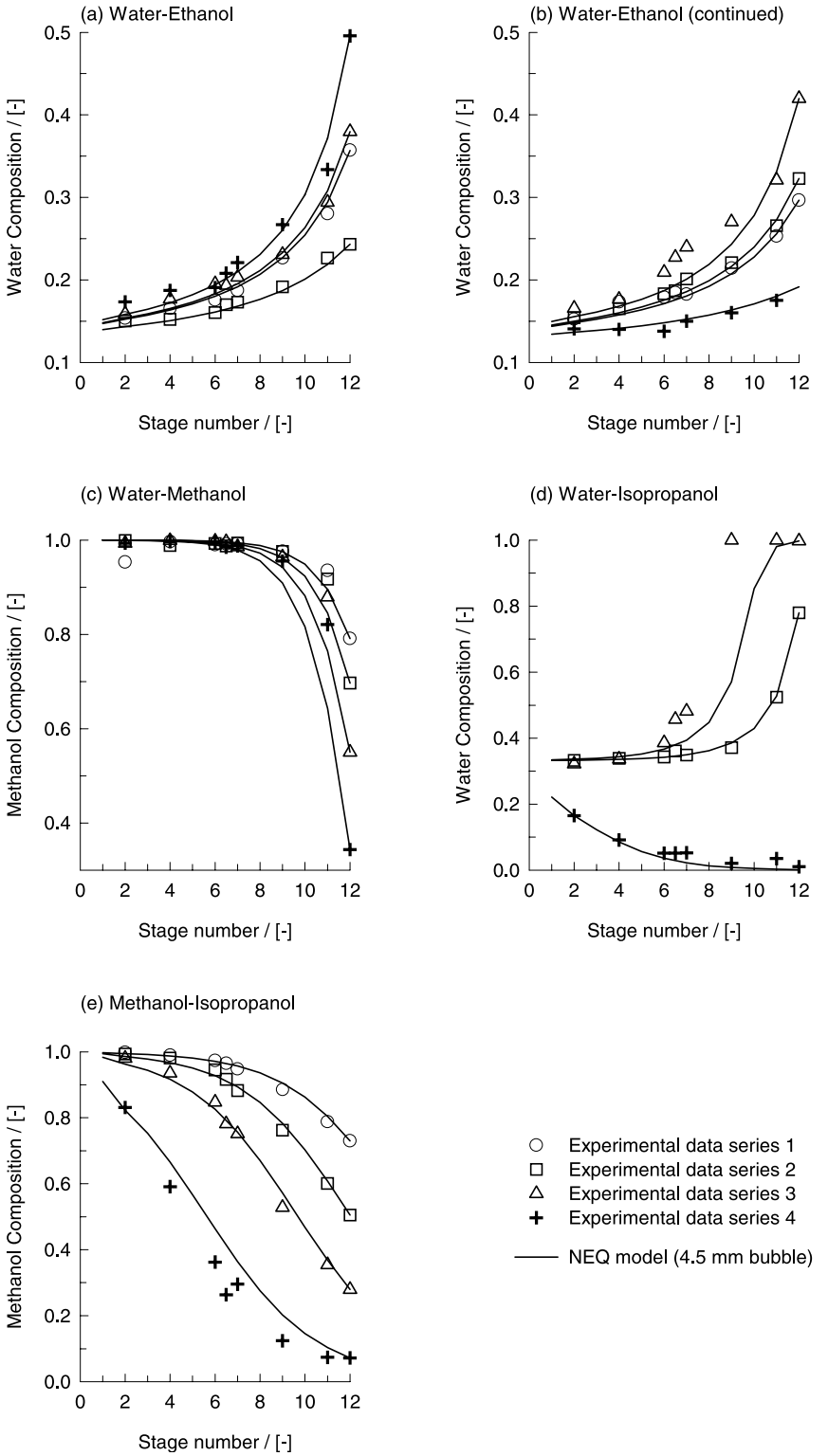
(a) Water-Ethanol
Water Composition / [-]
Stage number / [-]
(b) Water-Ethanol (continued)
Water Composition / [-]
Stage number / [-]
(c) Water-Methanol
Methanol Composition / [-]
Stage number / [-]
(d) Water-Isopropanol
Water Composition / [-]
Stage number / [-]
(e) Methanol-Isopropanol
Methanol Composition / [-]
Stage number / [-]
Experimental data series 1
Experimental data series 2
Experimental data series 3
Experimental data series 4
NEQ model (4.5 mm bubble)

Fig. 2.

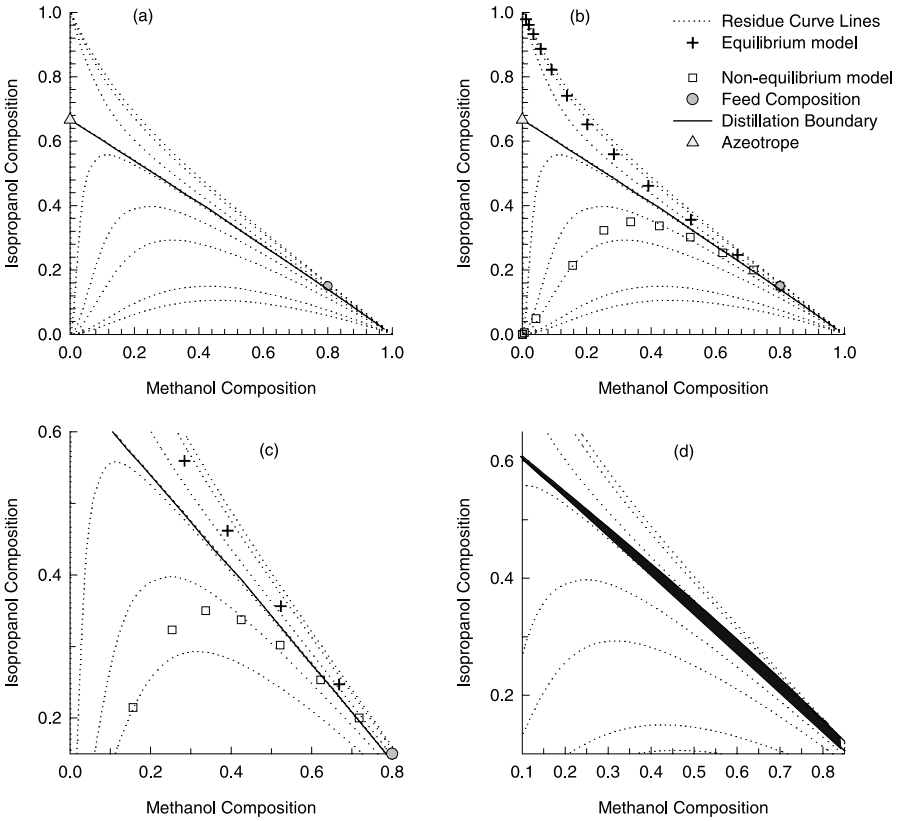

Fig. 3. (a) Residue curves for the system methanol (1)–isopropanol (2)–water (3). (b) and (c) compare EQ and NEQ distillation trajectories, showing same simulation drawn to different scales. In this simulation the total number of stages, including condenser and reboiler is 12. The column is operated at total reflux with no feed- and product-streams. The initial liquid composition is $x_1 = 0.8$, $x_2 = 0.15$ and fixed on stage 1 (condenser). For all feed compositions located in the shaded region in (d) boundary crossing is observed.

In order to understand the reasons behind the different trajectories followed by the EQ and NEQ models, we present information on the component vapour phase mole fraction driving forces, $y_i^* - y_{i,\mathrm{E}}$ in Fig. 4(a) and (b) we present the values of the component Murphree point efficiencies, E_i calculated on the basis of the multicomponent mass transfer theory presented above:

$$E_i = \frac{y_{i,\mathrm{L}} - y_{i,\mathrm{E}}}{y_i^* - y_{i,\mathrm{E}}}, i = 1,2,3 \tag{19}$$

We note that the component efficiencies of the individual components are all significantly different. These differences are to be traced to the differences in the vapour diffusivities of the binary pairs in the mixture (the interphase mass transfer process is controlled by vapour phase transport). For the component of intermediate volatility, isopropanol, we note that Murphree point efficiency shows a strong variation along the column. On stage 6 the efficiency is low (about 40%) and on the stage 7 this value increases to about 90%. The reason for this strong variation is to be found in the driving force of isopropanol which approaches vanishingly small values on stages 6 and 7; see Fig. 4(a). The transfer of isopropanol is strongly dictated by the transfer of the other two species, water and methanol.

We performed several simulations with the different feed compositions lying above the distillation boundary. For all feed compositions located in the dark shaded region shown in Fig. 3(d) we

observed that the NEQ model predicts that the straight line boundary will be crossed.

2.2. Water–ethanol–acetone system

Now we analyse the system: water (1)–ethanol (2)–acetone (3) that has one binary azeotrope, as indicated in Fig. 5(a). The boundary is almost a straight line and divides the composition triangle into two regions. We carried out total reflux simulations of a 12-stage column with a feed composition of $x_1 = 0.035$, $x_2 = 0.3$. For the chosen feed composition, which is located to the left of the distillation boundary, the EQ and NEQ trajectories are seen to follow completely different composition trajectories; see Fig. 5(b). The EQ trajectory gets progressively richer in ethanol as we move from the condenser downwards to the reboiler. The NEQ trajectory gets progressively richer in water as we move from the condenser downwards to the reboiler. The straight-line boundary crossing, observed with the NEQ model, is forbidden according to literature guidelines [9].

The difference in the EQ and NEQ column trajectories can be traced to the differences in the Murphree efficiencies of the three components, shown in Fig. 6(b). The differences in the component efficiencies can be traced to the differences in the values of the diffusivities of the binary pairs in the vapour phase (the transfer resistance in the liquid phase is negligible). The efficiency of ethanol assumes negative values on stage 10 and on stage 11 the efficiency value exceeding unity. This strange variation of the ethanol component efficiency is to be attributed to the component driving force of ethanol which has vanishingly small values on these stages; see Fig. 6(a). On stages 10 and 11 the transfer of ethanol is dictated by the transfer of the other two components in the mixture due to multicomponent coupling effects [21].

We performed several simulations with the feed compositions located to the left of the distillation boundary. For all feed compositions falling within the dark shaded region shown in Fig. 5(c), the NEQ model anticipates that the distillation boundary will be crossed from the left side.

2.3. Water–methanol–methylacetate system

Consider the system: water (1)–methanol (2)–methylcetate (3) for which the residue curve maps are shown in Fig. 7(a) for the region in which the liquid phase is homogeneous (there is a region of liquid-liquid phase splitting towards the right side of the triangular diagram; this is not considered in our analysis below. This system has two binary azeotropes and the distillation boundary is curved. Fig. 7(b) compares EQ and NEQ distillation trajectories in a 12-stage column for total

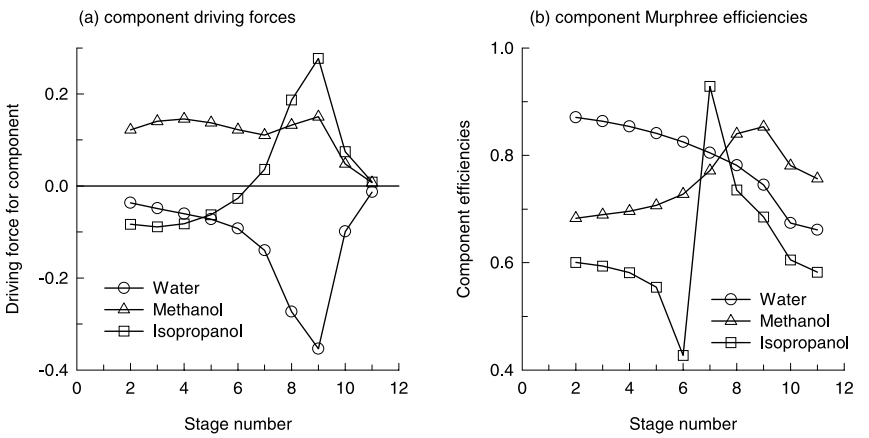

Fig. 4. (a) Component driving forces and (b) Murphree component efficiencies for the system methanol (1)–isopropanol (2)–water (3). The values correspond to the total reflux simulation whose initial liquid composition is $x_1 = 0.8$, $x_2 = 0.15$ and fixed on stage 1 (condenser).

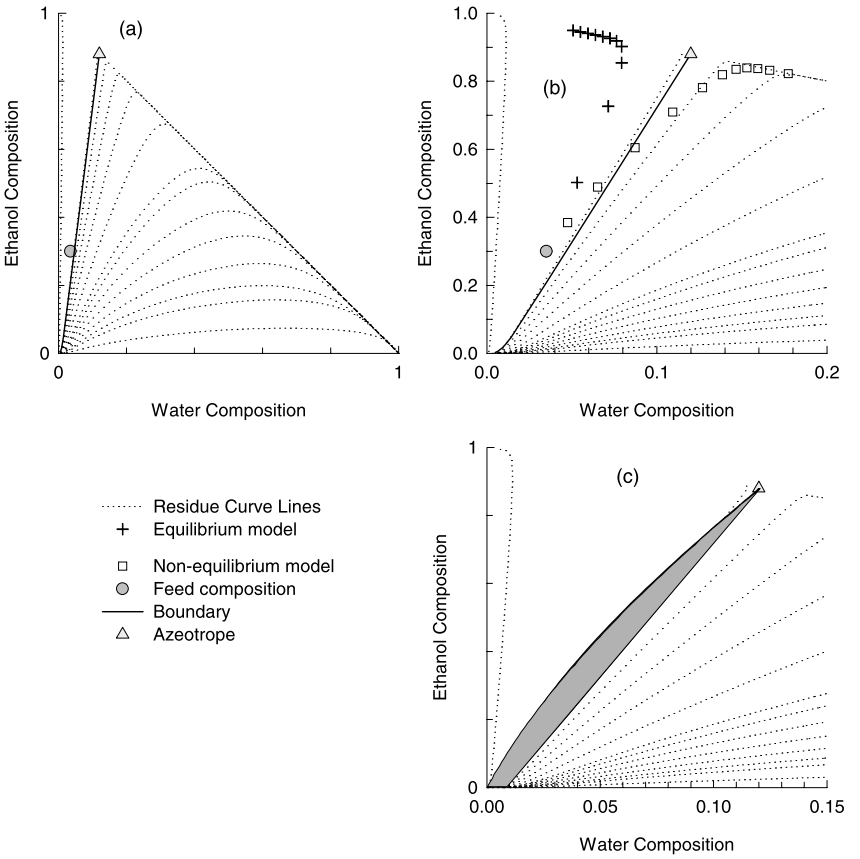

Fig. 5. (a) Residue curves for the system water (1)–ethanol (2)–acetone (3). (b) Compares EQ and NEQ distillation trajectories. In this simulation the total number of stages is 12. The column is operated at total reflux with no feed- and product-streams The initial liquid composition is $x_1 = 0.035$, $x_2 = 0.3$ and fixed on stage 1 (condenser). For all feed compositions located in the shaded region in (c) boundary crossing is observed.

reflux operation with the liquid composition leaving the condenser taken to be $x_1 = 0.044$, $x_2 = 0.2$. The feed is located on the concave side of the boundary. We find that the EQ and NEQ column trajectories move in different directions away from the condenser downwards; see Fig. 7(b). The EQ model predicts that the column gets progressively richer in methylacetate as we move down to the reboiler. The NEQ model, on the other hand, anticipates that the column gets progressively richer in water. Furthermore, we note that the NEQ trajectory crosses the distillation boundary. The difference in the EQ and NEQ column trajectories can be traced to the differences in the Murphree efficiencies of the three components, shown in Fig. 8(b). The differences in the component efficiencies can be traced to the differences in the values of the diffusivities of the binary pairs in the vapour phase (the transfer resistance in the liquid phase is negligible). The efficiency of methylacetate assumes a value below zero on stage 7 and is higher than 100% on stage 8. This strange variation of the methylacetate component efficiency is to be attributed to its component driving force which changes sign between stages 7 and 8; see Fig. 8 (a). On stages 7 and 8 the transfer of methylacetate is dictated by the transfer of the other two components in the mixture due to multicomponent coupling effects [21].

3. Conclusions

The following major observations and conclusions can be drawn.

- The EQ and NEQ models may predict completely different composition trajectories in ternary azeotropic distillation.
- For the methanol–isopropanol–water and water–ethanol–acetone systems, the NEQ model has been shown to be capable of crossing straight-line distillation boundaries. In the literature it is remarked that straight-line distillation boundaries cannot be crossed; this conclusion is restricted in its applicability to EQ models.

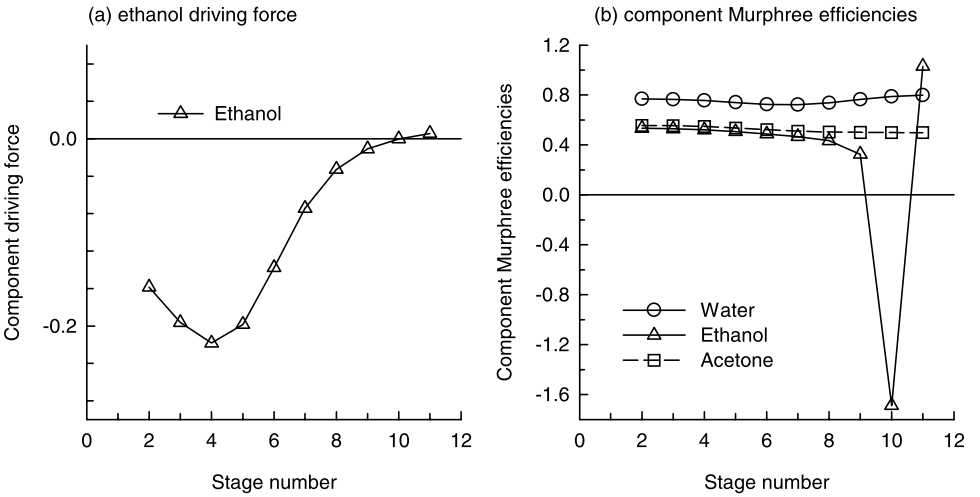

Fig. 6. (a) Ethanol driving force and (b) Murphree component efficiencies for the system water (1)–ethanol (2)–acetone (3). The values correspond to the total reflux simulation whose initial liquid composition is $x_1 = 0.035$, $x_2 = 0.3$ and fixed on stage 1 (condenser).

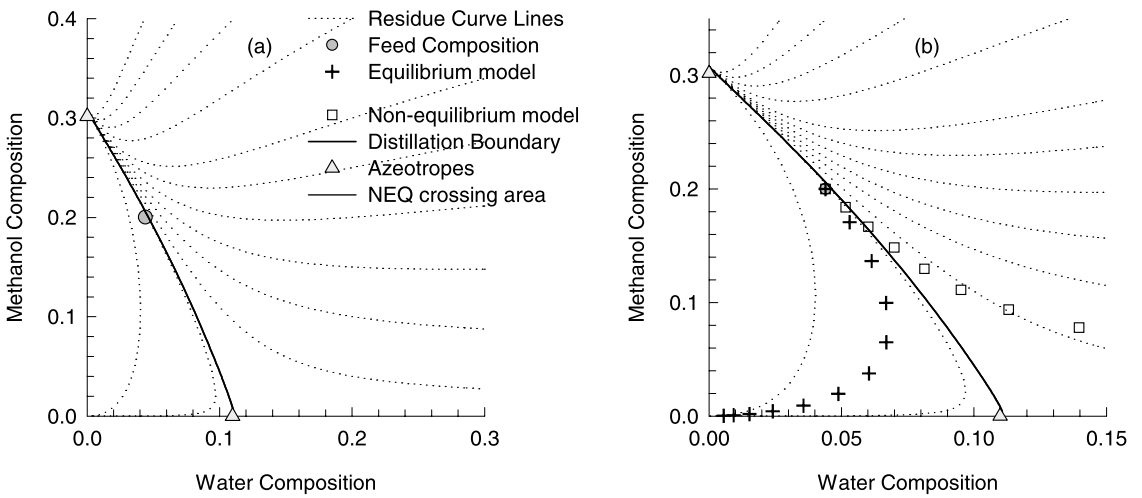

Fig. 7. (a) Residue curves for the system water (1)–methanol (2)–methylacetate (3). (b) Compares EQ and NEQ distillation trajectories. The total number of stages, including condenser and reboiler is 12. The column is operated at total reflux with no feed- and product-streams. The initial liquid composition is $x_1 = 0.044$, $x_2 = 0.2$ and fixed on stage 1 (condenser). For all feed compositions located in the shaded region in (c) boundary crossing is observed.

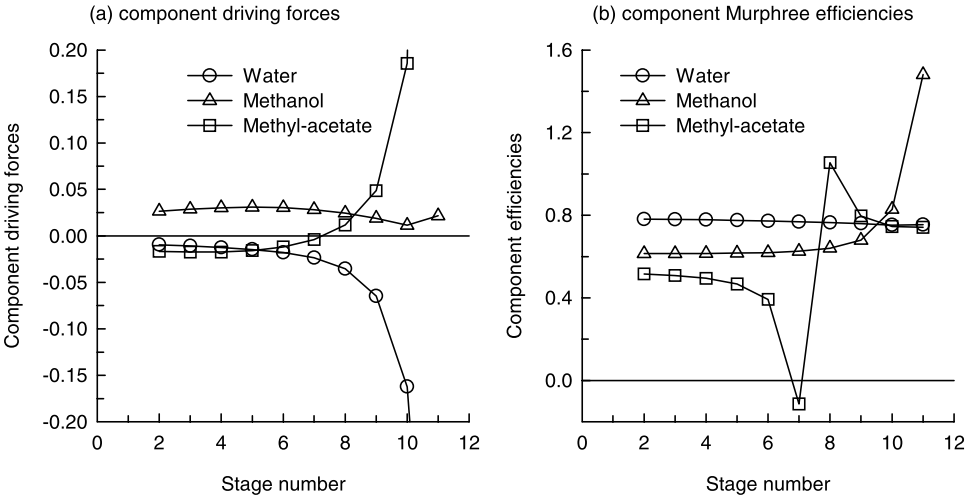

Fig. 8. (a) Component driving forces and (b) Murphree efficiencies for the system water (1)–methanol (2)–methylacetate (3). The values correspond to the total reflux simulation whose initial liquid composition is $x_1 = 0.044$, $x_2 = 0.2$ and fixed on stage 1 (condenser).

- For the systems water–methanol–methylcetate system, with the feed located on the *concave* side of a curved distillation boundary, the NEQ model trajectories are seen to be capable of crossing the boundary. The EQ model, in sharp contrast does not anticipate this boundary crossing phenomenon.

Our simulations demonstrate that the literature guidelines regarding boundary crossing do not have general validity. Boundary crossing phenomenon could also be influenced by interphase mass transfer. A straight-line boundary can be crossed. Separation strategies in practice are influenced by boundary crossing effects.

Acknowledgements

The authors acknowledges a grant *Programma-subsidie* from the Netherlands Organisation for Scientific Research (NWO) for development of novel concepts in reactive separations technology. The authors are grateful to R. Taylor and H. Kooijman for providing the code to *ChemSep*, which was used in this study after appropriate modification to include the rigid bubble model.

References

[1] J.G. Stichlmair, J.R. Fair, Distillation Principles and Practice, Wiley-VCH, New York, 1998.
[2] M.F. Doherty, M.F. Malone, Conceptual Design of Distillation Systems, McGraw-Hill, New York, 2001.
[3] S. Widagdo, W.D. Seider, Azeotropic distillation, A.I.Ch.E. J. 42 (1996) 96–130.
[4] J.P. Knapp, M.F. Doherty, A new pressure-swing-distillation process for separating homogeneous azeotropic mixtures, Ind. Eng. Chem. Res. 31 (1992) 346–357.
[5] H.N. Pham, M.F. Doherty, Design and synthesis of azeotropic distillation. 2. Residue curve maps, Chem. Eng. Sci. 45 (1990) 1837–1843.
[6] V. Julka, M.F. Doherty, Geometric behavior and minimum flows for nonideal multicomponent distillation, Chem. Eng. Sci. 45 (1990) 1801–1822.
[7] D. Barbosa, M.F. Doherty, The simple distillation of homogeneous reactive mixtures, Chem. Eng. Sci. 43 (1988) 541–550.
[8] Z.T. Fidkowski, M.F. Doherty, M.F. Malone, Feasibility of separations for distillation of nonideal ternary mixtures, A.I.Ch.E. J. 39 (1993) 1303–1321.
[9] S.G. Levy, D.B. van Dongen, M.F. Doherty, Design and synthesis of homogeneous azeotropic distillation. 2. Minimum reflux calculations for nonideal and azeotropic columns, Ind. Eng. Chem. Fundament. 24 (1985) 463–474.
[10] O.M. Wahnschafft, J.W. Koehler, A.W. Westerberg, Homogeneous azeotropic distillation—analysis of separation feasibility and consequences for entrainer selection and column design, Comp. Chem. Eng. 18 (1994) S31–S35.

[11] O.M. Wahnschafft, J.W. Koehler, E. Blass, A.W. Westerberg, The product composition regions of single-feed azeotropic distillation-columns, Ind. Eng. Chem. Res. 31 (1992) 2345–2362.
[12] B.S. Bossen, S.B. Joergensen, R. Gani, Simulation design and analysis of azeotropic distillation operations, Ind. Eng. Chem. Res. 32 (1993) 620–633.
[13] L. Laroche, N. Bekiaris, H.W. Andersen, M. Morari, The curious behavior of homogeneous azeotropic distillation — implications for entrainer selection, A.I.Ch.E. J. 38 (1992) 1309–1328.
[14] F.J.L. Castillo, D.Y.C. Thong, G.P. Towler, Homogeneous azeotropic distillation. 2. Design procedure for sequences of columns, Ind. Eng. Chem. Res. 37 (1998) 998–1008.
[15] E. Rev, Crossing of valleys, ridges and simple distillation boundaries by distillation in homogeneous ternary mixtures, Ind. Eng. Chem. Res. 31 (1992) 893–901.
[16] Y. Li, H. Chen, J. Liu, Composition profile of an azeotropic continuous distillation with feed composition on a ridge or in a valley, Ind. Eng. Chem. Res. 38 (1999) 2482–2484.
[17] S. Pelkonen, R. Kaesemann, A. Gorak, Distillation lines for multicomponent separation in packed columns: theory and comparison with experiment, Ind. Eng. Chem. Res. 36 (1997) 5392–5398.
[18] S. Pelkonen, A. Gorak, A. Ohligschläger, R. Kaesemann, Experimental study of multicomponent distillation in packed columns, Chem. Eng. Process 40 (2001) 235–243.
[19] G. Ronge, Überprüfung unterschiedelicher Modelle für den Stoffaustausch bei der Rektifikation in Packungskolonnen. Fortschritt-Berichte VDI Verfahrenstechnik No. 390, Düsseldorf, 1995.
[20] R. Krishna, J.A. Wesselingh, The Maxwell–Stefan approach to mass transfer, Chem. Eng. Sci. 52 (1997) 861–911.
[21] R. Taylor, R. Krishna, Multicomponent Mass Transfer, Wiley, New York, 1993.
[22] R. Baur, A.P. Higler, R. Taylor, R. Krishna, Comparison of equilibrium stage and non-equilibrium stage models for reactive distillation, Chem. Eng. J. 76 (2000) 33–47.
[23] R. Krishnamurthy, R. Taylor, Nonequilibrium stage model of multicomponent separation processes, A.I.Ch.E. J. 32 (1985) 449–465.
[24] R. Taylor, H.A. Kooijman, J.S. Hung, A second generation nonequilibrium model for computer-simulation of multicomponent separation processes, Comp. Chem. Eng. 18 (1994) 205–217.
[25] R. Baur, R. Taylor, R. Krishna, J.A. Copati, Influence of mass transfer in distillation of mixtures with a distillation boundary, Chem. Eng. Res. Design Trans. I. Chem. E. 77 (1999) 561–565.
[26] J.A. Wesselingh, R. Krishna, Mass Transfer in Multicomponent Mixtures, Delft University Press, Delft, 2000.
[27] F.J.L. Castillo, G.P. Towler, Influence of multicomponent mass transfer on homogeneous azeotropic distillation, Chem. Eng. Sci. 53 (1998) 963–976.
[28] J.L. Gmehling, U. Onken, Vapor-Liquid Equilibrium Data Collection, Dechema, Frankfurt, 1977.
[29] H.D. Mendelson, The prediction of bubble terminal velocities from wave theory, A.I.Ch.E.J. 13 (1967) 250–253.
[30] R. Krishna, M.I. Urseanu, J.M. van Baten, J. Ellenberger, Wall effects on the rise of single gas bubbles in liquids, Int. Comm. Heat Mass Transfer 26 (1999) 781–790.